

See discussions, stats, and author profiles for this publication at: <https://www.researchgate.net/publication/280581479>

# Varying Electronic Structures of Dirosmium Complexes from Noninnocently Behaving Anthraquinone-Derived Bis-chelate Ligands

ARTICLE *in* INORGANIC CHEMISTRY · JULY 2015

Impact Factor: 4.76 · DOI: 10.1021/acs.inorgchem.5b01017 · Source: PubMed

---

READS

16

## 5 AUTHORS, INCLUDING:



Abhishek Mandal

Indian Institute of Technology Bombay

6 PUBLICATIONS 20 CITATIONS

[SEE PROFILE](#)



Anita Drozdz

Universität Stuttgart

9 PUBLICATIONS 25 CITATIONS

[SEE PROFILE](#)



Brigitte Schwederski

Universität Stuttgart

77 PUBLICATIONS 1,102 CITATIONS

[SEE PROFILE](#)

## Varying Electronic Structures of Diosmium Complexes from Noninnocently Behaving Anthraquinone-Derived Bis-chelate Ligands

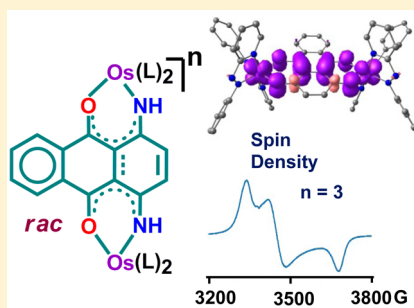
Abhishek Mandal,<sup>†</sup> Anita Grupp,<sup>‡</sup> Brigitte Schwederski,<sup>‡</sup> Wolfgang Kaim,<sup>\*,‡</sup> and Goutam Kumar Lahiri<sup>\*,†</sup>

<sup>†</sup>Department of Chemistry, Indian Institute of Technology Bombay, Powai, Mumbai 400076, India

<sup>‡</sup>Institut für Anorganische Chemie, Universität Stuttgart, Pfaffenwaldring 55, D-70550 Stuttgart, Germany

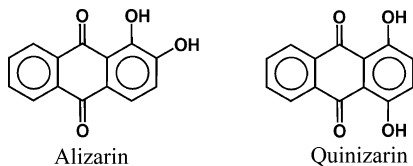
### S Supporting Information

**ABSTRACT:** The new compounds  $[(\text{bpy})_2\text{Os}^{\text{II}}(\mu-\text{L}_1^{2-})\text{Os}^{\text{II}}(\text{bpy})_2](\text{ClO}_4)_2$  (**[1]**) ( $\text{ClO}_4)_2$  and  $[(\text{pap})_2\text{Os}^{\text{II}}(\mu-\text{L}_1^{2-})\text{Os}^{\text{II}}(\text{pap})_2](\text{ClO}_4)_2$  (**[2]**) ( $\text{ClO}_4)_2$  ( $\text{H}_2\text{L}_1 = 1,4$ -dihydroxy-9,10-antraquinone, bpy = 2,2'-bipyridine, and pap = 2-phenylazopyridine) and  $[(\text{bpy})_2\text{Os}^{\text{II}}(\mu-\text{L}_2^{2-})\text{Os}^{\text{II}}(\text{bpy})_2](\text{ClO}_4)_3$  (**[3]**) ( $\text{ClO}_4)_3$  and  $[(\text{pap})_2\text{Os}^{\text{II}}(\mu-\text{L}_2^{2-})\text{Os}^{\text{II}}(\text{pap})_2](\text{ClO}_4)_2$  (**[4]**) ( $\text{ClO}_4)_2$  ( $\text{H}_2\text{L}_2 = 1,4$ -diamino-9,10-antraquinone) have been analytically identified as the *meso* and *rac* diastereoisomers, respectively. The paramagnetic **[3]** ( $\text{ClO}_4)_3$  was also characterized by crystal structure determination. In  $\text{CD}_3\text{CN}$  solution, **[3]** ( $\text{ClO}_4)_3$  displays rather narrow but widely split ( $13 > \delta > -8$  ppm) resonances in the  $^1\text{H}$  NMR spectrum, yet no EPR signal was observed down to 120 K. Cyclic voltammetry and differential pulse voltammetry reveal several accessible redox states on oxidation and reduction, showing that the replacement of 1,4-oxido by imido donors causes cathodic shifts and that the substitution of bpy by the stronger  $\pi$ -accepting pap ligands leads to a strong increase of redox potentials. Accordingly, system **[3]<sup>n</sup>** with the lowest (2+/3+) potential was synthetically obtained in the mono-oxidized (3+) form. The (3+) intermediates display small comproportionation constants  $K_c$  of about  $10^3$  and long-wavelength near-infrared absorptions; an EPR signal with appreciable *g* splitting (1.84, 1.96, and 2.03) was only observed for **[3]<sup>3+</sup>**, which exhibits the smallest spin density on the osmium centers. An oxidation state formulation  $[\text{Os}^{\text{III}}(\mu-\text{L}^{3-})\text{Os}^{\text{III}}]^{3+}$  with some  $[\text{Os}^{\text{II}}(\mu-\text{L}^{2-})\text{Os}^{\text{III}}]^{3+}$  contribution was found to best describe the electronic structures. UV-vis-NIR absorption spectra were recorded for all accessible states by OTTLE spectroelectrochemistry and assigned on the basis of TD-DFT calculations. These results and additional EPR measurements suggest rather variegated oxidation state situations, e.g., the pap ligands competing with the bridge L for electrons, while the oxidation produces mixed spin systems with variable metal/ligand contributions.



### INTRODUCTION

9,10-Antraquinones are widely found in industrial processes, in natural products, and in medicinal chemistry.<sup>1</sup> In addition, the useful redox activity<sup>2a</sup> and the metal-chelating capacity of 1,2-disubstituted (cf. alizarin) or 1,4-disubstituted hydroxyl (quinizarin,  $\text{H}_2\text{L}_1$ )<sup>2b–h</sup> or amino derivatives ( $\text{H}_2\text{L}_2$ ) have long been known. In the case of ruthenium coordination compounds,<sup>3</sup> remarkable oxidation state ambiguities can occur due to the availability of  $\text{Ru}^{\text{II,III,IV}}$  and  $\text{L}^{(0)-(4)}$  states of the components. The latter can be represented by structure formulas as shown in Scheme 1.



Less work has been devoted to corresponding osmium compounds, although osmium also adopts the II, III, and IV oxidation states readily. However, the more facile oxidation of Os versus corresponding Ru systems has to be considered, as have the effects of the much higher spin-orbit coupling for the

Sd element, leading to the emergence of absorption bands from otherwise forbidden transitions and resulting in strongly deviating *g* factors from the free electron value of 2.0023 in the EPR spectra of paramagnetic species.<sup>4</sup>

The present study describes four new compounds **[1]**–( $\text{ClO}_4)_2$ , **[2]**–( $\text{ClO}_4)_2$ , **[3]**–( $\text{ClO}_4)_3$ , and **[4]**–( $\text{ClO}_4)_2$  (Scheme 2), of which **[3]**–( $\text{ClO}_4)_3$  could be characterized crystallographically. Several other experimental/computational lines of investigation were applied to elucidate the nontrivial variations in the electronic structures, viz, voltammetric characterization (CV and DPV) of accessible members of the individual redox series, the EPR response of paramagnetic states as related to calculated spin densities, and UV-vis-NIR spectroscopic information with assignments based on TD-DFT calculation results for electronic transitions.

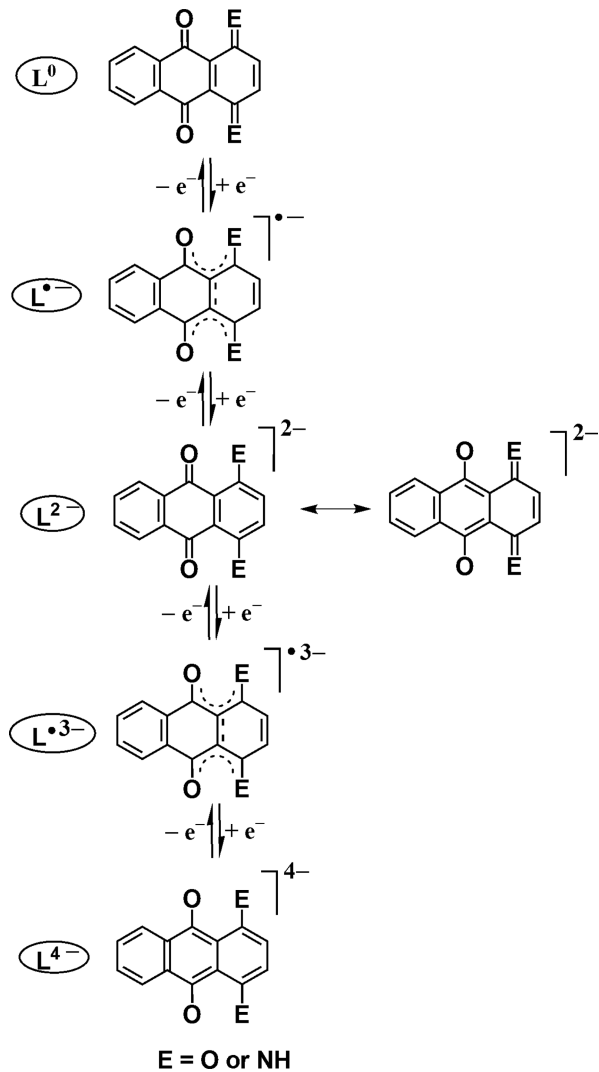
The present study allows for several kinds of comparison, viz, between O,O and O,NH coordination of the anthraquinone ligands, between complexes with moderately  $\pi$ -accepting bpy and strongly  $\pi$ -accepting pap ancillary ligands,<sup>5</sup> between the osmium system **[3]**–( $\text{ClO}_4)_3$  and related diruthenium species

Received: May 6, 2015

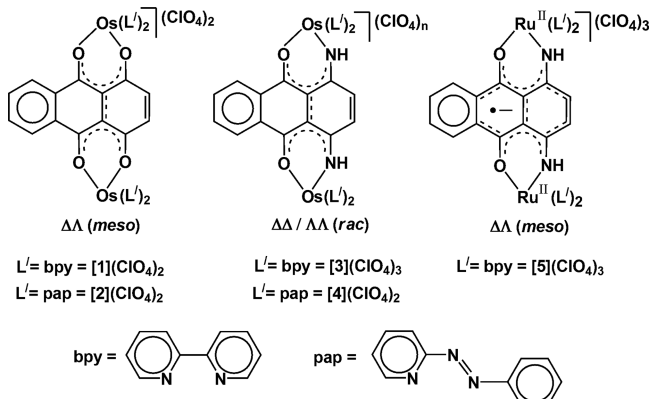
Published: July 31, 2015



Scheme 1. Representation of Ligand Oxidation States



Scheme 2. Representation of the Complexes

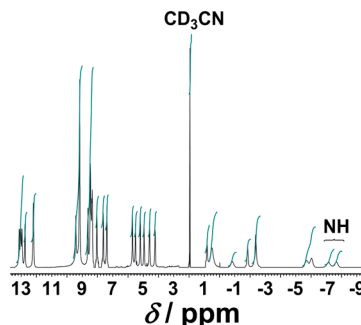


$[(\text{bpy})_2\text{Ru}^{\text{II}}(\mu-\text{L}_2^{\bullet-})\text{Ru}^{\text{II}}(\text{bpy})_2](\text{ClO}_4)_3$  (*meso*:  $[\mathbf{5}](\text{ClO}_4)_3$ ), and between *meso* and *rac* diastereoisomers at the computational level (DFT).<sup>3a</sup>

## RESULTS AND DISCUSSION

**Synthesis and Characterization.** The compounds (Scheme 2) were obtained by reacting *cis*- $\text{Os}(\text{bpy})_2\text{Cl}_2$ <sup>6a</sup> and

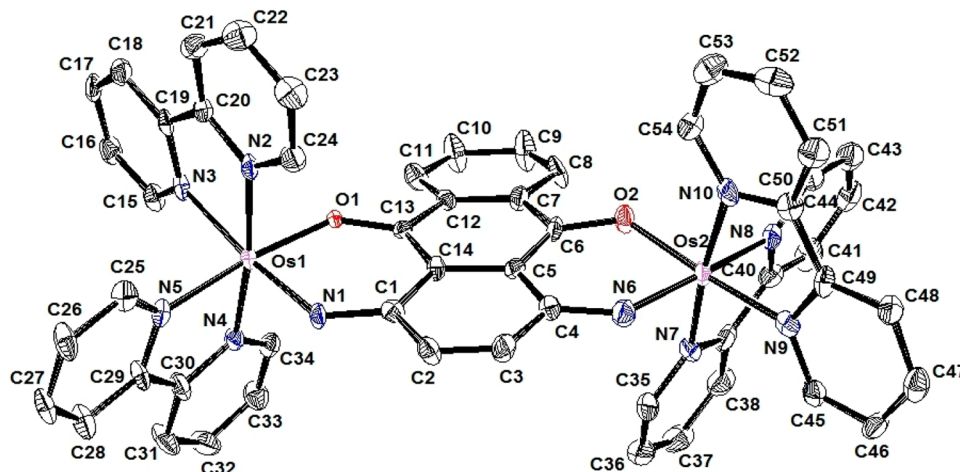
*cis-trans-cis*- $\text{Os}(\text{pap})_2\text{Cl}_2$ <sup>6b</sup> ( $\text{bpy} = 2,2'$ -bipyridine;  $\text{pap} = 2$ -phenylazopyridine) with the ligands 1,4-dihydroxy-9,10-anthraquinone and 1,4-diamino-9,10-anthraquinone. Only one of the two possible diastereoisomers (*meso* ( $\Delta\Lambda$ ) and *rac* ( $\Delta\Delta/\Lambda\Lambda$ ))<sup>3a</sup> due to the presence of two chiral metal centers was obtained in each case after chromatographic purification. Analytical and mass spectrometric data confirm the composition (Experimental Section and Figure S1, Supporting Information), while  $^1\text{H}$  NMR spectroscopy (Experimental Section, Figure 1, and Figure S2, Supporting Information) in

Figure 1.  $^1\text{H}$  NMR spectrum of  $[\mathbf{3}](\text{ClO}_4)_3$  in  $\text{CD}_3\text{CN}$ .

conjunction with X-ray crystallography has been used to identify the diastereoisomers (*meso* for  $1^{2+}$  and  $2^{2+}$ , and *rac* for  $3^{3+}$  and  $4^{2+}$ ) on the basis of symmetry and number of observed resonances. The comparatively low oxidation potential (Ox1 =  $-0.14$  V versus SCE, Table 1 and Figure 3, see later) has facilitated the stabilization of the tricationic form,  $3^{3+}$  under atmospheric reaction conditions.

While the isolated diamagnetic compounds  $[\mathbf{1}](\text{ClO}_4)_2$ ,  $[\mathbf{2}](\text{ClO}_4)_2$ , and  $[\mathbf{4}](\text{ClO}_4)_2$  exhibit the expected  $^1\text{H}$  NMR resonance signals in the  $6.5 < \delta < 9.5$  "aromatic" chemical shift range in  $\text{DMSO}-d_6$  or  $\text{CD}_3\text{CN}$  solution (Figure S2, Supporting Information), the paramagnetic and structurally characterized (cf. below)  $[\mathbf{3}](\text{ClO}_4)_3$  in its *rac* form displays rather narrow resonance lines in a much wider range between  $-8$  and  $+13$  ppm (Figure 1). The related ruthenium complex ( $[\mathbf{5}](\text{ClO}_4)_3$  as the *meso* isomer) exhibits a similar effect, however, with more broadened resonance lines.<sup>3a</sup> This broadening of the NMR resonances in  $5^{3+}$  agrees with the low metal spin density (0.256) and the well observed EPR spectrum for the ruthenium case versus high metal spin density (0.416) in  $3^{3+}$  leading to the EPR silent situation due to the rapid relaxation process via the involvement of strong spin-orbit coupling of  $\text{Os}^{\text{III}}$  ( $\lambda = 3000$   $\text{cm}^{-1}$  (Os), 1000  $\text{cm}^{-1}$  (Ru)) (cf. below). While the most upfield shifted signals are assigned to the NH protons which also reflects a positive spin density of 0.086 at each N as calculated by DFT (see below), a similar argument holds to attribute downfield shifted resonances to the protons at the 2,3-positions of the anthraquinone ligand with spin densities of  $-0.008$ . This splitting due to paramagnetic contact shift<sup>3b,7</sup> is not unexpected; nevertheless, the fairly good resolution suggests favorable relaxation conditions for NMR detection. Conversely, the compound is EPR silent in the range down to 120 K, suggesting a rapid relaxation not unexpected for dinuclear paramagnetic compounds of osmium<sup>4,8</sup> with its rather high spin-orbit coupling of about 3000  $\text{cm}^{-1}$ .<sup>9</sup>

**Crystal Structure Analysis.** In contrast to the previously reported diruthenium analogue of  $[\mathbf{3}](\text{ClO}_4)_3$  which was isolated as the *meso* isomer,<sup>3a</sup> the diosmium complex was

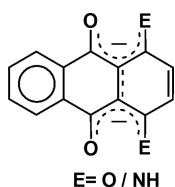


**Figure 2.** Molecular structure of the complex trication in  $[3](\text{ClO}_4)_3 \cdot 2\text{CH}_3\text{CN}$ . Ellipsoids are drawn at 50% probability level. Solvent molecules and hydrogen atoms are removed for clarity.

obtained in the *rac* configuration as the bis(acetonitrile) solvate. Tables S1 and S2 (*Supporting Information*) list crystallographic data and selected bond parameters, and Figure 2 illustrates the molecular structure of the trication. The NH functions in the trication  $3^{3+}$  are engaged in weak hydrogen bonding<sup>10</sup> to the  $\text{CH}_3\text{CN}$  nitrogen atoms ( $\text{NH} \cdots \text{N}$  3.153 Å, angle  $\text{NHN}$  145°) (Figure S3, *Supporting Information*).

While the CC distances in the aromatic ring are typical at 1.40 Å and the bond between C2 and C3 is short at 1.315(11) Å, the other C–C bond lengths in the bridging ligand are relatively long (1.42–1.46 Å) (Table S2, *Supporting Information*). Using Scheme 1, the bridge structure parameters within the complex trication can be interpreted as those of a dianion, agreeing also with a formulation of the bridge as involving two  $\beta$ -ketiminato-type chelate arrangements (Scheme 3).

### Scheme 3. Representation of the Double $\beta$ -Ketiminato-Type Chelating Bridge



The metal bonds to NH are shorter than those to the less basic O atoms of the bridge (Tables S2–S11, *Supporting Information*). DFT calculations overestimate these bond lengths, a not unexpected result.<sup>11</sup>

**Electrochemistry.** Cyclic and differential pulse voltammetry reveal several reversibly accessible redox states on oxidation and reduction (Figure 3 and Table 1). The substitution of the 1,4-oxido by the 1,4-imido donors causes cathodic shifts in agreement with the higher electronegativity of O versus NH. This effect must be stronger for electron transfers which involve the bridging ligand, such as the first and second reduction. However, the replacement of bpy by the stronger  $\pi$ -accepting pap ligands causes significant anodic shifts, which are largest (~1.0 V) for those electron transfers (Ox1, Ox2) involving the metals. As a consequence, the redox system  $3''$  with the lowest

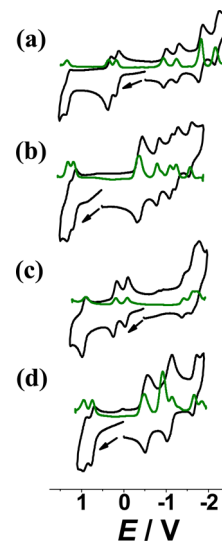


**Figure 3.** Cyclic (black) and differential pulse (green) voltammograms of (a)  $[1](\text{ClO}_4)_2$ , (b)  $[2](\text{ClO}_4)_2$ , (c)  $[3](\text{ClO}_4)_2$  after prereduction, and (d)  $[4](\text{ClO}_4)_2$  in  $\text{CH}_3\text{CN}/0.1 \text{ M Et}_4\text{NClO}_4$  versus SCE; the scan rate is  $100 \text{ mV s}^{-1}$ .

( $2+/3+$ ) potential was isolated in the mono-oxidized ( $3+$ ) form.

A conspicuous common feature of the four redox systems is the occurrence of two slightly split oxidation waves which define the ( $3+$ ) intermediate with comproportionation constants  $K_c$  between  $10^{2.4}$  and  $10^{4.7}$  (Table 1). For the diruthenium complex *meso*-[5](ClO<sub>4</sub>)<sub>3</sub> related to *rac*-[3](ClO<sub>4</sub>)<sub>3</sub>, the corresponding  $K_c$  is distinctly higher at  $10^{7.3}$ .<sup>3a</sup> This significant difference can be traced to the donor function of the bridge which favors a “hole transfer” pathway of valence exchange.<sup>8</sup> In other words, the reduction of M<sup>III</sup> to M<sup>II</sup> is more difficult to perform for M=Os than for M=Ru. Hence, electron transfer from the bridging ligand to the M<sup>III</sup> center is more endergonic for M=Os, leading to weaker electronic interaction between the metal centers in the diosmium case. The following EPR and spectroelectrochemical results will serve to establish the electronic structures of these intermediates and of other electrogenerated charge states.

**EPR Spectroscopy.** The EPR spectra of osmium compounds, even of those with ligand based spin, are strongly

Table 1. Electrochemical Data<sup>a</sup>

	$E^\circ_{298}/V (\Delta E/\text{mV})^b$								$K_c^{c,d}$
	Ox3	Ox2	Ox1	Red1	Red2	Red3	Red4	Red5	
1 <sup>2+</sup>	1.33 (100)	0.34 (80)	0.16 (80)	0.97 (70)	1.27 (60)	1.82 (110)	2.20 (120)		$10^{3.1}$
2 <sup>2+</sup>		1.29 (70)	1.15 (60)	0.40 (120)	0.83 (60)	1.13 (60)	1.27 (80)	1.59 (80)	$10^{2.4}$
3 <sup>3+</sup>	0.85 (90)	0.14 (80)	0.14 (70)	1.47 (70)	1.74 (210)				$10^{4.7}$
4 <sup>2+</sup>		0.92 (60)	0.73 (80)	0.54 (70)	1.09 (130)	1.68 (100)			$10^{3.2}$

<sup>a</sup>From cyclic voltammetry in  $\text{CH}_3\text{CN}/0.1 \text{ M Et}_4\text{NClO}_4$  at  $100 \text{ mVs}^{-1}$ . <sup>b</sup>Potential in V versus SCE; peak potential differences  $\Delta E/\text{mV}$  are in parentheses. <sup>c</sup>Comproportionation constant from  $RT \ln K_c = nF(\Delta E)$ . <sup>d</sup> $K_c$  between Ox1 and Ox2.

affected by the very high spin–orbit coupling constant of the 5d element in its various oxidation states.<sup>4,8,9</sup> As a result, considerable g factor deviations from the free electron value of 2.0023 can be expected (a relativistic effect);<sup>12</sup> however, another frequent consequence is the rapid relaxation leading to broadened and sometimes vanishing resonance signals (EPR silence), as reported, e.g., for  $[(\text{bpy})_2\text{Os}(\mu\text{-adcR})\text{Os}(\text{bpy})_2]^{3+}$ , adcR = azodicarbonyl derivative,  $[\text{R(O)CNNC(O)R}]^n$ .<sup>4</sup>

Remarkably, monocationic and tricationic species display quite different EPR responses, as supported by their spin density plots (Figures 4 and 5–8) and as summarized in Table 2 and Table S12 (Supporting Information).

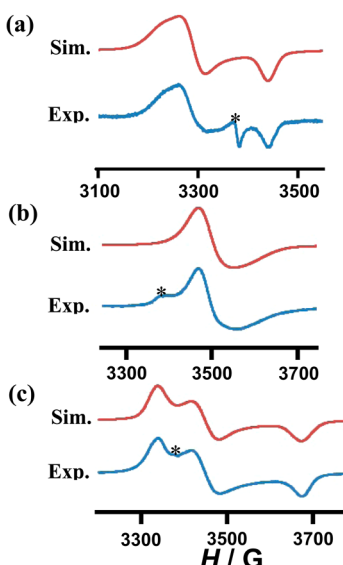


Figure 4. EPR spectra of (a)  $1(\text{ClO}_4)_2$ , (b)  $2(\text{ClO}_4)_2$  after electrolytic reduction, and (c)  $4(\text{ClO}_4)_2$  after oxidation at a platinum electrode in  $\text{CH}_2\text{Cl}_2/0.1 \text{ M Bu}_4\text{NPF}_6$  at  $120 \text{ K}$ , together with corresponding simulations using data from Table 2. (\*: cavity signal.)

The one-electron reduction of  $1^{2+}$  in  $\text{CH}_2\text{Cl}_2/0.1 \text{ M Bu}_4\text{NPF}_6$  produces a monocation with an isotropic g factor of 2.019, observable at room temperature. This value, together with the relatively small g factor splitting  $g_1\text{-}g_3$  of 0.131 in the frozen state at  $120 \text{ K}$  suggests a detectable but small metal contribution to the singly occupied molecular orbital (SOMO) (Tables S13–S40, Supporting Information).

The calculated Mulliken spin densities of only 0.030 on each Os in  $1^+$  (Figures 5 and Table S12, Supporting Information) agree with the experiment, in that the unpaired electron resides mainly in the bridge. Oxidation to  $1^{3+}$  is calculated to produce a spin density of 0.296 at each metal with only 0.436 remaining at the bridge (Table S12, Supporting Information), and accordingly, no EPR signal was detected.

For the oxidation to  $2^{3+}$  a similar situation is encountered due to the combined metal spin densities of 0.493. Reduction to  $2^+$  produces a barely split EPR signal at about  $g = 1.92$  at low temperatures, suggesting ligand-based spin but enhanced relaxation. In agreement with the experiment, the calculated spin densities reveal pap-based spin ( $\text{pap}^{\bullet-}$ ) due to the superior  $\pi$ -acceptor properties of that ancillary ligand<sup>5</sup> (not a mere “spectator!”) with vanishing metal contributions. While the g factor splitting is hardly detectable, the deviation to  $g < 2$  is well-known for such kinds of radical anion ligand systems with Ru<sup>II</sup> or Os<sup>II</sup>.<sup>4,8,13</sup> The absence of an EPR signal at ambient temperatures is attributed to the presence of several equivalent pap coligands, which leads to several close-lying states and thus rapid relaxation for the monoreduced species, despite largely ligand-based spin.

Both  $3^{3+}$  (the isolated form) and  $3^+$  were found to be EPR-silent under the measurement conditions. Large metal spin densities (0.416 combined) for  $3^{3+}$  and a calculated bridge/bpy mixed spin distribution with rapid EPR relaxation for  $3^+$  are held responsible.

In contrast to the other (3+) ions, the electrogenerated  $4^{3+}$  exhibits an EPR spectrum at  $120 \text{ K}$  (Figure 4). The reason may be sought in the relatively low spin densities on the metals (0.156 on each Os) as compared to a value of 0.676 for the bridging  $\pi$ -system. The large g factor splitting of  $g_1\text{-}g_3 = 0.190$ , the deviation of g to lower values, and the absence of a signal at room temperature confirm the small but effective influence from the heavy metal centers. Combining these results with the structural information for the related  $3^{3+}$  allows us to propose a description combining  $[\text{Os}^{\text{III}}(\mu\text{-L}^{\bullet-})\text{Os}^{\text{III}}]^{3+}$  with  $[\text{Os}^{\text{II}}(\mu\text{-L}^{2-})\text{Os}^{\text{III}}]^{3+}$  for the (3+) ions, with varying contributions from the metal and from the bridge. Whereas the latter, mixed-valent formulation<sup>4</sup> yields spin density for the metal centers, the former would provide ligand spin density if the three-spin arrangement follows the pattern  $\uparrow\ldots\downarrow\uparrow$  for a noncoplanar situation.<sup>14</sup> The corresponding diruthenium system (studied in the meso form) shows still lower metal spin densities of 0.256 and thus a higher ligand spin density of 0.752; accordingly, its EPR spectrum is well observable at  $110 \text{ K}$  with a smaller g anisotropy  $g_1\text{-}g_3 = 0.104$  and more broadened  $^1\text{H}$  NMR resonances.<sup>3a</sup>

In fact, a comparison of spin densities (which is supported by EPR) reveals that the osmium system  $3^{3+}$  exhibits a higher metal spin density (0.416) than the ruthenium analogue  $5^{3+}$  (0.256), the O,O ligated systems  $1^{3+}$  and  $2^{3+}$  exhibit higher metal spin densities (0.592 and 0.493) than the O,NH chelated analogues  $3^{3+}$  and  $4^{3+}$  (0.416 and 0.313), and the bpy containing complexes  $1^{3+}$  and  $3^{3+}$  (0.592 and 0.416) exhibit higher spin densities than the corresponding pap ligated analogues ( $2^{3+}, 4^{3+}$ ) (0.493, 0.313), all reflecting higher stability of the trivalent metal (d<sup>5</sup>) configuration (Table S12, Supporting Information).

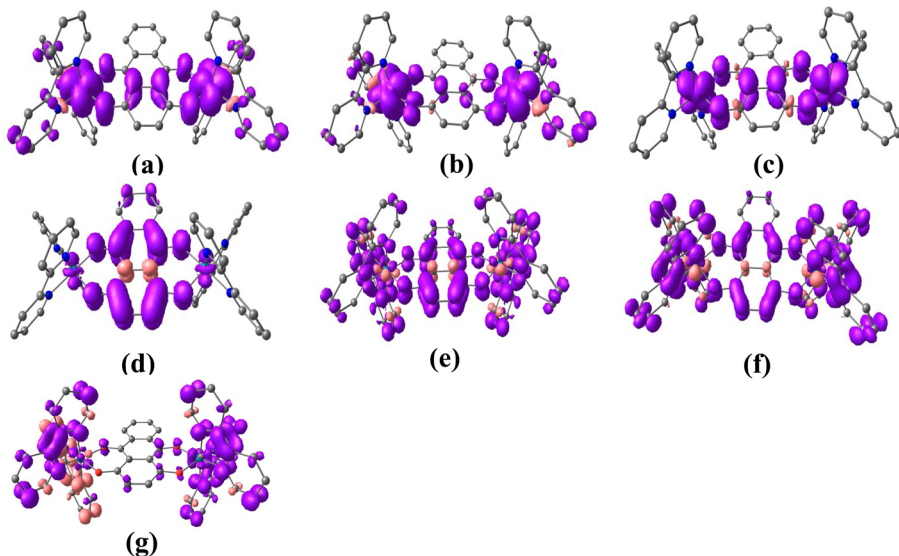


**Figure 5.** Spin density representations of (a)  $\mathbf{1}^{5+}$  ( $S = 3/2$ ), (b)  $\mathbf{1}^{4+}$  ( $S = 1$ ), (c)  $\mathbf{1}^{3+}$  ( $S = 1/2$ ), (d)  $\mathbf{1}^+$  ( $S = 1/2$ ), (e)  $\mathbf{1}^-$  ( $S = 1$ ), (f)  $\mathbf{1}^-$  ( $S = 3/2$ ), and (g)  $\mathbf{1}^{2-}$  ( $S = 1$ ).

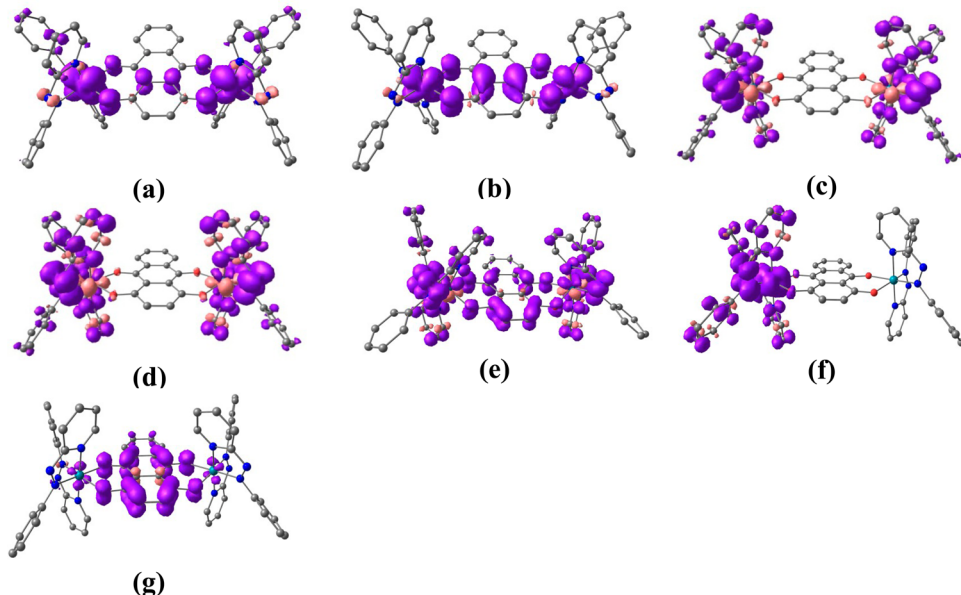


**Figure 6.** Spin density representations of (a)  $\mathbf{2}^{4+}$  ( $S = 1$ ), (b)  $\mathbf{2}^{3+}$  ( $S = 1/2$ ), (c)  $\mathbf{2}^+$  ( $S = 1/2$ ), (d)  $\mathbf{2}^-$  ( $S = 1$ ), (e)  $\mathbf{2}^-$  ( $S = 3/2$ ), (f)  $\mathbf{2}^{2-}$  ( $S = 1$ ), and (g)  $\mathbf{2}^{3-}$  ( $S = 1/2$ ).

Reduction to  $\mathbf{4}^+$  did not produce an EPR response at 120 K. Since pap-based spin is calculated for this form (Figure 8 and Table S12, Supporting Information), we may invoke the same arguments as outlined above for the  $\mathbf{2}^+$  ion: The presence of several equivalent pap coligands (and of multiply reducible  $\mu$ -L) can lead to several close-lying states and thus rapid relaxation in spite of mostly ligand-based spin.

The above arguments from combined structural and EPR studies in conjunction with DFT calculations suggest the following redox series for the complexes (Scheme 4).

**UV–Vis–NIR Spectroelectrochemistry.** The availability of several, even high charge states for the series of osmium compounds prompted us to study the absorption spectra in the UV, vis, and NIR ranges by spectroelectrochemistry in an optically transparent thin layer electrolysis (OTTLE) cell. The spectra are displayed in Figure 9 and Figures S4–S6

(Supporting Information), and the experimental data (Table S41, Supporting Information) are compared with results from TD-DFT calculations in Tables S42–S45, Supporting Information.

The central ( $2+$ ) states which exist over a relatively wide potential range (Figure 3) exhibit low-energy absorptions between 700 and 1000 nm (Tables S42–S45, Supporting Information), attributed to MLCT transitions (to  $\mu$ -L for  $\mathbf{1}^{2+}$  or pap for  $\mathbf{2}^{2+}$ ) or to (bridging ligand)-to-(ancillary ligand) charge transfer processes ( $\mathbf{3}^{2+}$  and  $\mathbf{4}^{2+}$ ).

On oxidation to the ( $3+$ ) intermediate discussed above, there are near-infrared absorptions emerging in the 1000–2000 nm range (Figure 9 and Figures S4–S6 and Tables S42–S45, Supporting Information). These remarkable long-wavelength features, at least two in each case, are best characterized as MLCT transitions, although they involve considerably mixed

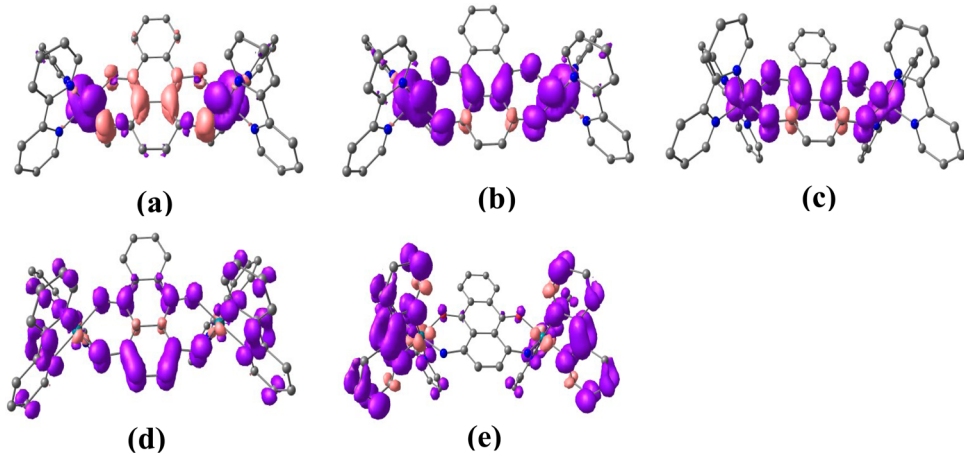


**Figure 7.** Spin density representations of (a)  $3^{5+}$  ( $S = 1/2$ ), (b)  $3^{4+}$  ( $S = 1$ ), (c)  $3^{3+}$  ( $S = 1/2$ ), (d)  $3^+$  ( $S = 1/2$ ), and (e)  $3$  ( $S = 1$ ).

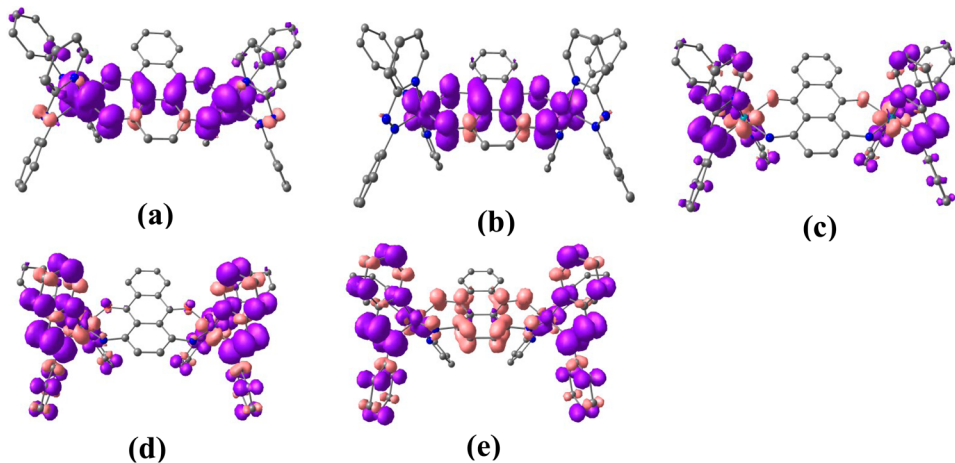


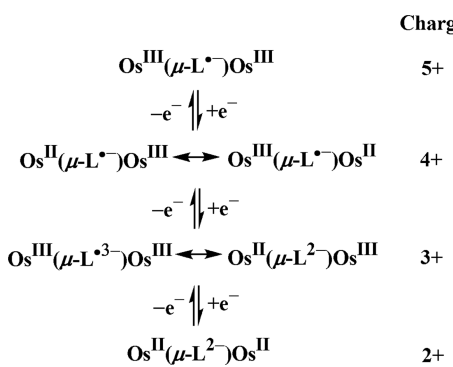
**Figure 8.** Spin density representations of (a)  $4^{4+}$  ( $S = 1$ ), (b)  $4^{3+}$  ( $S = 1/2$ ), (c)  $4^+$  ( $S = 1/2$ ), (d)  $4$  ( $S = 1$ ), and (e)  $4^-$  ( $S = 1/2$ ).

**Table 2. EPR Parameters for  $1^n$ ,  $2^n$ , and  $4^n$  in  $\text{CH}_2\text{Cl}_2/0.1 \text{ M Bu}_4\text{NPF}_6$  at 120 K**

complex	$g_1$	$g_2$	$g_3$	$\langle g \rangle^a$	$\Delta g^b$
$1^+$	2.100	2.060	1.969	2.044 <sup>c</sup>	0.131
$2^+$	1.94	1.94	1.89	1.923	0.05
$4^{3+}$	2.032	1.964	1.842	1.948	0.190

<sup>a</sup> $\langle g \rangle = \{(1/3)(g_1^2 + g_2^2 + g_3^2)\}^{1/2}$ . <sup>b</sup> $\Delta g = g_1 - g_3$ . <sup>c</sup> $g_{\text{iso}} = 2.019$  at 295 K.

**Scheme 4. Suggested Oxidation States**



orbitals in agreement with the spin density results. Radical-bridged dimetal complexes as well as mixed-valent species can exhibit NIR absorptions of high intensity,<sup>15</sup> and the latter plays

a major role in  $1^{3+}$  which reveals strong contributions from metal-to-metal charge transfer (MMCT). The absence of strongly donating imino functions and strongly accepting pap coligands favors the metal–metal interaction in this case.

The formal description of the (4+) state as involving radical ion-bridged mixed-valent metals has been invoked before for diruthenium species,<sup>3a,16</sup> which also exhibit intense near-infrared absorptions with mixed MLCT/MMCT character. The  $S = 1$  ground state is well separated here from the  $S = 0$  state by about  $2000 \text{ cm}^{-1}$  (Tables S46–S49, Supporting Information).

Metal-to-ligand charge transfer is dominant for the low-energy transitions of the (5+) ion observable for system  $3^n$ , the osmium(III) centers serving as donors, whereas the radical anion form of the bridge acts as an acceptor. The  $S = 1/2$  ground state calculated is a consequence of metal–ligand antiferromagnetic coupling.<sup>14</sup>

The monocations also reveal near IR absorptions which can be attributed to LLCT or intraligand (IL) transitions, in agreement with EPR and DFT information on ligand localized spin. Neutral species and anionic states were accessible for  $1^n$  and  $2^n$ , reflecting the higher electronegativity of O versus NH. In agreement with EPR and spin density results, the target orbital of long-wavelength transitions for  $2^{n+}$  and  $4^{n+}$  is the low-lying  $\pi^*(\text{pap})$  MO.

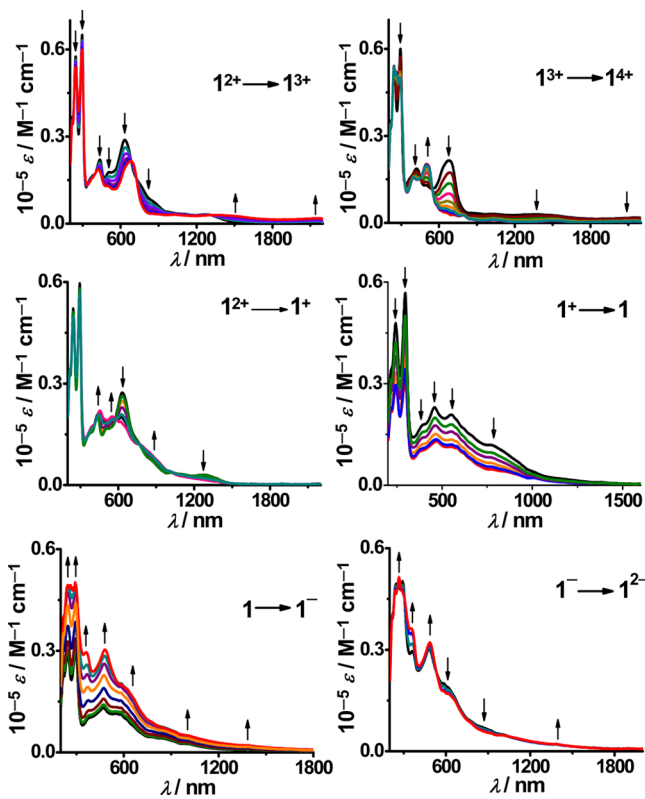


Figure 9. UV-vis-NIR spectroelectrochemistry of  $\mathbf{1}^n$  ( $n = 4^+$ ,  $3^+$ ,  $2^+$ ,  $+$ ,  $0$ ,  $1^-$ , and  $2^-$ ) in  $\text{CH}_3\text{CN}/0.1 \text{ M } \text{NBu}_4\text{PF}_6$ .

## CONCLUSIONS

We have described a series of potentially mixed-valent dinuclear complexes bridged by redox-active ligands. Osmium has been chosen as a heavy metal from the iron group with its frequently stable paramagnetic  $\text{Os}^{\text{III}}$  ( $5d^5$ ) oxidation state and a very high spin-orbit coupling constant. The ligands are bis-chelating 1,4-disubstituted 9,10-anthraquinones, classical components of natural and industrial dyes. A radical complex structure was determined crystallographically for the *rac* configurated diastereoisomer  $[\mathbf{3}](\text{ClO}_4)_3$  which exhibits narrow but contact-shifted  $^1\text{H}$  NMR resonances and remains EPR silent down to 120 K. This intermediate as well as other ( $3^+$ ) ions exhibit rather small comproportionation constants of  $K_c = 10^2\text{--}10^{4.7}$  when compared to those of ruthenium analogues, suggesting the hole transfer mechanism<sup>8</sup> for valence exchange via the bridge. In other words, the reduction of  $\text{M}^{\text{III}}$  to  $\text{M}^{\text{II}}$  is more difficult to perform for  $\text{M}=\text{Os}$  than for  $\text{M}=\text{Ru}$ . Hence, electron transfer from the bridging ligand to the  $\text{M}^{\text{III}}$  center is more endergonic for  $\text{M}=\text{Os}$ , leading to weaker electronic interaction between the metal centers in the diosmium case. A large number of reversibly accessible other oxidation states has been analyzed by UV-vis-NIR spectroelectrochemistry and EPR within the corresponding redox series. The combined experimental evidence is supported by DFT and TD-DFT calculations to yield a consistent description from comparing variations in donor atoms ( $\text{O}, \text{NH}$ ) of the bridge, ancillary ligands (bpy, pap), and metals (Os, Ru). Higher oxidation states can be reached for the osmium compounds than for ruthenium analogues. In the ( $3^+$ ) series with  $\text{O}, \text{NH}$  donor ligand, the spin density on the metal is higher for the Os example ( $3^{3+}$ ) than for the related Ru analogue  $\mathbf{5}^{3+}$ , for the bpy compounds  $\mathbf{1}^{3+}$  and  $3^{3+}$  in comparison to the pap analogues  $2^{3+}$  and  $4^{3+}$ , and for the

$\text{O}, \text{O}$  chelate systems  $1^{3+}$  and  $2^{3+}$  versus the  $\text{O}, \text{NH}$  analogues  $3^{3+}$  and  $4^{3+}$ . As a result, the  $3^{3+}$  ion is the most stable and even isolable case in that series, whereas the  $4^{3+}$  species is the only one to exhibit EPR response at 120 K due to small metal contributions to the SOMO. Spectroelectrochemistry showed absorbance of most states in the near-infrared region because both anthraquinone radical ions and diosmium mixed-valent configurations lead to low-energy transitions. The redox series in Scheme 4 has been deduced from the combined experimental and computational results, demonstrating the excellent potential of anthraquinone derivatives as electron transfer active components<sup>2a</sup> and as noninnocent ligands in nontrivial, challenging combinations of three different suspect components (metal, bridging, and terminal ligands).

## EXPERIMENTAL SECTION

**Materials.** The precursor complexes *cis*- $\text{Os}(\text{bpy})_2\text{Cl}_2$ <sup>6a</sup> and *cis-trans-cis*- $\text{Os}(\text{pap})_2\text{Cl}_2$ <sup>6b</sup> were prepared according to procedures reported in the literature. The ligands 1,4-dihydroxy-9,10-anthraquinone and 1,4-diamino-9,10-anthraquinone were purchased from Alfa Aesar. Other chemicals and solvents were of reagent grade and used as received. For spectroscopic and electrochemical studies, HPLC grade solvents were used.

**Physical Measurements.** The electrical conductivity of the solution was checked by using an autoranging conductivity meter (Toshcon Industries, India). The EPR measurements were made in a two-electrode capillary tube<sup>13</sup> with an X-band (9.5 GHz) Bruker system ESP300 spectrometer. Cyclic voltammetric and differential pulse voltammetric measurements of the complexes in the isolated native state were done using a PAR model 273A electrochemistry system. A glassy carbon working platinum wire auxiliary electrode and saturated calomel reference electrode (SCE) were used in a standard three-electrode configuration with tetraethylammonium perchlorate (TEAP) as the supporting electrolyte (substrate concentration  $\approx 10^{-3}$  M; standard scan rate 100 mV s<sup>-1</sup>). (Caution! Perchlorate salts are explosive and should be handled with care.) UV-vis-NIR spectroelectrochemical studies were performed in  $\text{CH}_3\text{CN}/0.1 \text{ M } \text{Bu}_4\text{NPF}_6$  at 298 K using an optically transparent thin-layer electrode (OTTLE) cell<sup>17</sup> mounted in the sample compartment of a J&M TIDAS spectrophotometer. All spectroelectrochemical experiments were carried out under a dinitrogen atmosphere.  $^1\text{H}$ NMR spectra were recorded on a Bruker Avance III 400 MHz spectrometer. The elemental analyses were recorded on a PerkinElmer 240C elemental analyzer. Electrospray mass spectral measurements were done on a Micromass Q-ToF mass spectrometer.

**Preparation of Complexes.** *Synthesis of  $[\text{Os}_2(\text{bpy})_4(\mu-\text{L}_1^{2-})](\text{ClO}_4)_2$*  ( $[\mathbf{1}] (\text{ClO}_4)_2$ ). The starting complex *cis*- $\text{Os}(\text{bpy})_2\text{Cl}_2$  (100 mg, 0.18 mmol) and the ligand  $\text{H}_2\text{L}_1$  (21 mg, 0.09 mmol) were taken in 50 mL of 2:1  $\text{C}_2\text{H}_5\text{OH}/\text{H}_2\text{O}$  and then  $\text{NEt}_3$  (0.03 mL, 0.18 mmol) was added to the solution, followed by refluxing for 72 h under aerobic conditions. The solvent was removed, and the residue was moistened with a few drops of  $\text{CH}_3\text{CN}$ , followed by the addition of a saturated aqueous  $\text{NaClO}_4$  solution. After storing at 273 K overnight, the precipitate was filtered and washed with chilled water to remove excess  $\text{NaClO}_4$  and dried in vacuo over  $\text{P}_2\text{O}_{10}$ . The product was purified using a neutral alumina column, and the green complex  $[\mathbf{1}] (\text{ClO}_4)_2$  was eluted by a 2:1  $\text{CH}_3\text{CN}/\text{CH}_2\text{Cl}_2$  mixture. The solvent was removed to yield pure  $[\mathbf{1}] (\text{ClO}_4)_2$ . Yield, 81 mg (65%). MS (ESI+,  $\text{CH}_3\text{CN}$ ):  $m/z$   $[\mathbf{1}] \text{ClO}_4_2^+$  calcd, 1342.17; found, 1342.16.  $^1\text{H}$  NMR (400 MHz) in  $\text{DMSO}-d_6$  [ $\delta/\text{ppm}$  ( $J/\text{Hz}$ )]: 8.81 (m, 2H), 8.72 (m, 2H), 8.13 (m, 1H), 8.01 (m, 1H), 7.85 (m, 2H), 7.67 (m, 1H), 7.57 (m, 3H), 7.51 (m, 4H), 7.27 (d, 5, 1H), 7.1 (m, 1H), 7.06 (m, 1H). Anal. Calcd for  $\text{C}_{54}\text{H}_{38}\text{N}_8\text{O}_{12}\text{Cl}_2\text{Os}_2$ : C, 44.97; H, 2.66; N, 7.77; found, C, 44.72; H, 2.69; N, 7.64. Molar conductivity ( $\text{CH}_3\text{CN}$ ):  $\Lambda_M = 175 \Omega^{-1} \text{ cm}^2 \text{ M}^{-1}$ .

*Synthesis of  $[\text{Os}_2(\text{pap})_4(\mu-\text{L}_1^{2-})](\text{ClO}_4)_2$*  ( $[\mathbf{2}] (\text{ClO}_4)_2$ ). The starting complex *cis-trans-cis*- $\text{Os}(\text{pap})_2\text{Cl}_2$  (100 mg, 0.16 mmol) and the ligand  $\text{H}_2\text{L}_1$  (19 mg, 0.08 mmol) were taken in 50 mL of 1:1  $\text{C}_2\text{H}_5\text{OH}/\text{H}_2\text{O}$ ,

and then  $\text{NEt}_3$  (0.03 mL, 0.18 mmol) was added to the solution, followed by refluxing for 72 h under aerobic conditions. The solvent was removed, and the residue was moistened with a few drops of  $\text{CH}_3\text{CN}$ , followed by the addition of a saturated aqueous  $\text{NaClO}_4$  solution. After storing at 273 K overnight, the precipitate was filtered and washed with chilled water to remove excess  $\text{NaClO}_4$  and dried in vacuo over  $\text{P}_4\text{O}_{10}$ . The product was purified using a neutral alumina column, and the purple complex  $[2](\text{ClO}_4)_2$  was eluted by 1:1  $\text{CH}_3\text{CN}/\text{CH}_2\text{Cl}_2$  mixture. The solvent was removed to yield pure  $[2](\text{ClO}_4)_2$ . Yield, 67 mg (54%). MS (ESI $^+$ ,  $\text{CH}_3\text{CN}$ ):  $m/z$   $\{[2]\text{ClO}_4\}^+$  calcd, 1451.21; found, 1451.22.  $^1\text{H}$  NMR (400 MHz) in  $\text{CD}_3\text{CN}$  [ $\delta/\text{ppm}$  ( $J/\text{Hz}$ )]: 8.68 (m, 1H), 8.63 (m, 1H), 8.11 (m, 1H), 7.9 (m, 3H), 7.49 (m, 1H), 7.38 (m, 3H), 7.25 (m, 4H), 7.15 (m, 2H), 7.07 (m, 1H), 6.80 (m, 2H), 6.73 (m, 2H); Anal. Calcd for  $\text{C}_{58}\text{H}_{42}\text{N}_{12}\text{O}_{12}\text{Cl}_2\text{Os}_2$ : C, 44.93; H, 2.73; N, 10.84; found, C, 44.82; H, 2.61; N, 10.73. Molar conductivity ( $\text{CH}_3\text{CN}$ ):  $\Lambda_M = 182 \Omega^{-1} \text{ cm}^2 \text{ M}^{-1}$ .

**Synthesis of  $[\text{Os}_2(\text{bpy})_4(\mu-\text{L}_2^-)](\text{ClO}_4)_3$  ( $[3](\text{ClO}_4)_3$ ).** The starting complex *cis*- $\text{Os}(\text{bpy})_2\text{Cl}_2$  (100 mg, 0.18 mmol) and the ligand  $\text{H}_2\text{L}_2$  (21 mg, 0.09 mmol) were taken in 50 mL of 2:1  $\text{C}_2\text{H}_5\text{OH}/\text{H}_2\text{O}$ , and then  $\text{NEt}_3$  (0.03 mL, 0.18 mmol) was added to the solution, followed by refluxing for 72 h under aerobic conditions. The solvent was removed, and the residue was moistened with a few drops of  $\text{CH}_3\text{CN}$ , followed by the addition of a saturated aqueous  $\text{NaClO}_4$  solution. After storing at 273 K overnight, the precipitate was filtered and washed with chilled water to remove excess  $\text{NaClO}_4$  and dried in vacuo over  $\text{P}_4\text{O}_{10}$ . The product was purified using a neutral alumina column, and the violet complex  $[3](\text{ClO}_4)_3$  was eluted by 1:50  $\text{CH}_3\text{OH}/\text{CH}_2\text{Cl}_2$  mixture. The solvent was removed to yield the pure  $[3](\text{ClO}_4)_3$ . Yield, 68 mg (51%). MS (ESI $^+$ ,  $\text{CH}_3\text{CN}$ ):  $m/z$   $\{[3]\text{ClO}_4\}_2^+$  calcd, 1440.20; found, 1440.19.  $^1\text{H}$  NMR (400 MHz) in  $\text{CD}_3\text{CN}$  [ $\delta/\text{ppm}$  ( $J/\text{Hz}$ )]: 13.1 (3H), 12.75 (1H), 12.22 (2H), 9.45 (2H), 9.15 (5H), 8.65 (2H), 8.4 (6H), 8.05 (1H), 7.65 (1H), 7.38 (1H), 5.75 (1H), 5.55 (1H), 5.2 (1H), 4.95 (1H), 4.6 (1H), 4.28 (1H), 1.15 (1H), 0.5 (2H), -0.85 (1H), -1.85 (1H), -2.38 (2H), -5.7 (1H), -6.05 (1H), -7.15 (1H, NH), -7.7 (1H, NH); Anal. Calcd for  $\text{C}_{54}\text{H}_{40}\text{N}_{10}\text{O}_{14}\text{Cl}_3\text{Os}_2$ : C, 42.12; H, 2.62; N, 9.10; found, C, 42.06; H, 2.54; N, 9.19. Molar conductivity ( $\text{CH}_3\text{CN}$ ):  $\Lambda_M = 290 \Omega^{-1} \text{ cm}^2 \text{ M}^{-1}$ .

**Synthesis of  $[\text{Os}_2(\text{pap})_4(\mu-\text{L}_2^-)](\text{ClO}_4)_2$  ( $[4](\text{ClO}_4)_2$ ).** The starting complex *cis-trans-cis*- $\text{Os}(\text{pap})_2\text{Cl}_2$  (100 mg, 0.16 mmol) and the ligand  $\text{H}_2\text{L}_2$  (19 mg, 0.08 mmol) were taken in 50 mL of 1:1  $\text{C}_2\text{H}_5\text{OH}/\text{H}_2\text{O}$ , and then  $\text{NEt}_3$  (0.03 mL, 0.18 mmol) was added to the solution, followed by refluxing for 72 h under aerobic conditions. The solvent was removed, and the residue was moistened with a few drops of  $\text{CH}_3\text{CN}$ , followed by the addition of a saturated aqueous  $\text{NaClO}_4$  solution. After storing at 273 K overnight, the precipitate was filtered and washed with chilled water to remove excess  $\text{NaClO}_4$  and dried in vacuo over  $\text{P}_4\text{O}_{10}$ . The product was purified using a neutral alumina column, and the reddish-brown complex  $[4](\text{ClO}_4)_2$  was eluted by a 2:1  $\text{CH}_3\text{CN}/\text{CH}_2\text{Cl}_2$  mixture. The solvent was removed to yield the pure  $[4](\text{ClO}_4)_2$ . Yield, 73 mg (59%). MS (ESI $^+$ ,  $\text{CH}_3\text{CN}$ ):  $m/z$   $\{[4]\text{ClO}_4\}^+$  calcd, 1449.24; found, 1449.24.  $^1\text{H}$  NMR (400 MHz) in  $\text{CD}_3\text{CN}$  [ $\delta/\text{ppm}$  ( $J/\text{Hz}$ )]: 8.68 (m, 1H), 8.63 (m, 1H), 8.11 (m, 1H), 7.9 (m, 3H), 7.49 (m, 1H), 7.38 (m, 3H), 7.25 (m, 4H), 7.15 (m, 2H), 7.07 (m, 1H), 6.80 (m, 2H), 6.73 (m, 2H); Anal. Calcd for  $\text{C}_{58}\text{H}_{44}\text{N}_{14}\text{O}_{10}\text{Cl}_2\text{Os}_2$ : C, 44.99; H, 2.86; N, 12.66; found, C, 44.85; H, 2.78; N, 12.71. Molar conductivity ( $\text{CH}_3\text{CN}$ ):  $\Lambda_M = 168 \Omega^{-1} \text{ cm}^2 \text{ M}^{-1}$ . (Caution! Perchlorate salts are explosive and should be handled with care.)

**Crystal Structure Determination.** Single crystals of  $[3](\text{ClO}_4)_3$  were grown by slow evaporation of its 1:1  $\text{CH}_3\text{CN}$ -toluene solution. X-ray diffraction data were collected using a Rigaku Saturn-724+ CCD single crystal diffractometer using  $\text{Mo}-\text{K}\alpha$  radiation. The data collection was evaluated by using the CrystalClear-SM Expert software. The data were collected by the standard  $\omega$ -scan technique. The structure was solved by direct methods<sup>18</sup> and refined by full matrix least-squares with SHELXL-97, refining on  $F^2$ .<sup>19</sup> All data were corrected for Lorentz and polarization effects, and all non-hydrogen atoms were refined anisotropically. The remaining hydrogen atoms

were placed in geometrically constrained positions and refined with isotropic temperature factors, generally  $1.2U_{eq}$  of their parent atoms. Hydrogen atoms were included in the refinement process as per the riding model. SQUEEZE was applied for one disordered perchlorate ion in the crystal of  $[3](\text{ClO}_4)_3 \cdot 2\text{CH}_3\text{CN}$ .

**Computational Details.** Full geometry optimizations were carried out using the density functional theory method at the (U)B3LYP level for 1<sup>n</sup> ( $n = 5+, 4+, 3+, +, 0, -, 2-$ ), 2<sup>n</sup> ( $n = 4+, 3+, +, 0, -, 2-, 3-$ ), 3<sup>n</sup> ( $n = 5+, 4+, 3+, +, 0, -, 2-$ ), 4<sup>n</sup> ( $n = 4+, 3+, +, 0, -, 2-, 3-$ ), and (R)B3LYP for 1<sup>2+</sup>, 2<sup>2+</sup>, 3<sup>2+</sup>, and 4<sup>2+</sup>.<sup>20</sup> All elements except osmium were assigned the 6-31G(d) basis set. The LanL2DZ basis set with effective core potential was employed for the osmium atom.<sup>21</sup> All calculations were performed with the Gaussian09 program package.<sup>22</sup> Vertical electronic excitations based on (U)B3LYP optimized geometries were computed using the time-dependent density functional theory (TD-DFT) formalism<sup>23</sup> in acetonitrile using the conductor-like polarizable continuum model (CPCM).<sup>24</sup> Chem3D<sup>1.7</sup><sup>25</sup> was used to calculate the fractional contributions of various groups to each molecular orbital. All of the calculated structures were visualized with ChemCraft.<sup>26</sup>

## ASSOCIATED CONTENT

### Supporting Information

X-ray crystallographic file in CIF format for  $[3](\text{ClO}_4)_3$ , mass spectra,  $^1\text{H}$  NMR, hydrogen bonding parameters, UV-vis-NIR spectroelectrochemistry, DFT optimized structures, crystal data, Mulliken spin densities, MO compositions, UV-vis-NIR spectroelectrochemical data, TD-DFT calculated electronic transitions, and energies. The Supporting Information is available free of charge on the ACS Publications website at DOI: [10.1021/acs.inorgchem.5b01017](https://doi.org/10.1021/acs.inorgchem.5b01017). CCDC-1055327 ( $[3](\text{ClO}_4)_3 \cdot 2\text{CH}_3\text{CN}$ ) contains the supplementary crystallographic data for this Article. These data can be obtained free of charge from The Cambridge Crystallographic Data Centre via [www.ccdc.cam.ac.uk/data\\_request/cif](http://www.ccdc.cam.ac.uk/data_request/cif).

## AUTHOR INFORMATION

### Corresponding Authors

(W.K.) E-mail: [kaim@iac.uni-stuttgart.de](mailto:kaim@iac.uni-stuttgart.de).  
(G.K.L.) E-mail: [lahiri@chem.iitb.ac.in](mailto:lahiri@chem.iitb.ac.in).

### Notes

The authors declare no competing financial interest.

## ACKNOWLEDGMENTS

Financial support received from the Department of Science and Technology, Council of Scientific and Industrial Research (fellowship to A.M.) New Delhi (India), the DAAD, FCI, and DFG (Germany) is gratefully acknowledged.

## REFERENCES

- Lown, J. W. *Pharmacol. Ther.* **1993**, *60*, 185–214.
- (a) Baghernejad, M.; Zhao, X.; Ørnsø, K. B.; Füeg, M.; Moreno-García, P.; Rudnev, A. V.; Kaliginedi, V.; Vesztergom, S.; Huang, C.; Hong, W.; Broekmann, P.; Wandlowski, T.; Thygesen, K. S.; Bryce, M. R. *J. Am. Chem. Soc.* **2014**, *136*, 17922–17925. (b) Lee, C. W.; Yuan, Z.; Ahn, K. D.; Lee, S. H. *Chem. Mater.* **2002**, *14*, 4572–4575.
- Carter, T. P.; Gillispie, G. D.; Connolly, M. A. *J. Phys. Chem.* **1982**, *86*, 192–196.
- (d) Ramakrishna, G.; Singh, A. K.; Palit, D. K.; Ghosh, H. N. *J. Phys. Chem. B* **2004**, *108*, 4775–4783.
- Breinl, W.; Friedrich, J.; Haarer, D. *J. Chem. Phys.* **1984**, *81*, 3915–3921.
- Gracia, L. G.; Rodriguez, L. C.; Ceba, M. R. *Talanta* **1997**, *44*, 75–83.
- Fabriciova, G.; Sanchez-Cortes, S.; Garcia-Ramos, J. V.; Miskovsky, P. *J. Raman Spectrosc.* **2004**, *35*, 384–389.
- Rouhani, S.; Salimi, S. *Prog. Color Colorants Coat.* **2008**, *1*, 11–17.
- (a) Mandal, A.; Agarwala, H.; Ray, R.; Plebst, S.; Momin, S. M.; Priego, J. L.; Jiménez-Aparicio, R.; Kaim, W.; Lahiri, G. K. *Inorg. Chem.*

- 2014, 53, 6082–6093. (b) Maji, S.; Sarkar, B.; Mobin, S. M.; Fiedler, J.; Urbanos, F. A.; Jimenez-Aparicio, R.; Kaim, W.; Lahiri, G. K. *Inorg. Chem.* **2008**, 47, 5204–5211. (c) Ghumaan, S.; Mukherjee, S.; Kar, S.; Roy, D.; Mobin, S. M.; Sunoj, R. B.; Lahiri, G. K. *Eur. J. Inorg. Chem.* **2006**, 2006, 4426–4441. (d) Gooden, V. M.; Dasgupta, T. P.; Gordon, N. R.; Sadler, G. G. *Inorg. Chim. Acta* **1998**, 268, 31–36.
- (4) Kaim, W.; Sarkar, B. *Coord. Chem. Rev.* **2013**, 257, 1650–1659.
- (5) Patra, S.; Sarkar, B.; Maji, S.; Fiedler, J.; Urbanos, F. A.; Jimenez-Aparicio, R.; Kaim, W.; Lahiri, G. K. *Chem. - Eur. J.* **2006**, 12, 489–498.
- (6) (a) Lay, P. A.; Sargeson, M.; Taube, H. *Inorg. Synth.* **1986**, 24, 291–299. (b) Ghosh, B. K.; Goswami, S.; Chakravorty, A. *Inorg. Chem.* **1983**, 22, 3358–3360.
- (7) (a) Kumbhakar, D.; Sarkar, B.; Maji, S.; Mobin, S. M.; Fiedler, J.; Urbanos, F. A.; Jiménez-Aparicio, R.; Kaim, W.; Lahiri, G. K. *J. Am. Chem. Soc.* **2008**, 130, 17575–11583. (b) Patra, S.; Sarkar, B.; Ghumaan, S.; Fiedler, J.; Kaim, W.; Lahiri, G. K. *Inorg. Chem.* **2004**, 43, 6108–6113. (c) Das, A.; Scherer, T.; Maji, S.; Mondal, T. K.; Mobin, S. M.; Urbanos, F. A.; Jiménez-Aparicio, R.; Kaim, W.; Lahiri, G. K. *Inorg. Chem.* **2011**, 50, 7040–7049. (d) Koiba, T.; Masuda, Y.; Shono, J.; Kawamoto, Y.; Hoshino, Y.; Hashimoto, T.; Natarajan, K.; Shimizu, K. *Inorg. Chem.* **2004**, 43, 6215–6223. (e) Eaton, D. R. *J. Am. Chem. Soc.* **1965**, 87, 3097–3102. (f) Palmer, R. A.; Fay, R. C.; Piper, T. S. *Inorg. Chem.* **1964**, 3, 875–881. (g) Holm, R. H.; Cotton, F. A. *J. Am. Chem. Soc.* **1958**, 80, 5658–5663. (h) Fay, R. C.; Piper, T. S. *J. Am. Chem. Soc.* **1963**, 85, 500–504. (i) Chen, J.-L.; Zhang, X.-U.; Zhang, L.-Y.; Shi, L.-X.; Chen, Z.-N. *Inorg. Chem.* **2005**, 44, 1037–1043.
- (8) Kaim, W.; Lahiri, G. K. *Angew. Chem., Int. Ed.* **2007**, 46, 1778–1796.
- (9) Weil, J. A.; Bolton, J. R.; Wertz, J. E. *Electron Paramagnetic Resonance*; Wiley: New York, 1994; pp 532–536.
- (10) Li, W. K.; Zhou, G. D.; Mak, T. C. W. *Advanced Structural Inorganic Chemistry*; IUCr: Oxford, 2008; p 404.
- (11) (a) Neese, F. *Coord. Chem. Rev.* **2009**, 253, 526–563. (b) Kepp, K. P. *Coord. Chem. Rev.* **2013**, 257, 196–209.
- (12) Autschbach, J. *J. Chem. Phys.* **2012**, 136, 150902.
- (13) Kaim, W.; Ernst, S.; Kasack, V. *J. Am. Chem. Soc.* **1990**, 112, 173–178.
- (14) Ye, S.; Sarkar, B.; Lissner, F.; Schleid, T.; van Slageren, J.; Fiedler, J.; Kaim, W. *Angew. Chem., Int. Ed.* **2005**, 44, 2103–2106.
- (15) Kaim, W. *Coord. Chem. Rev.* **2011**, 255, 2503–2513.
- (16) (a) Sarkar, B.; Patra, S.; Fiedler, J.; Sunoj, R. B.; Janardanan, D.; Mobin, S. M.; Niemeyer, M.; Lahiri, G. K.; Kaim, W. *Angew. Chem., Int. Ed.* **2005**, 44, 5655–5658. (b) Sarkar, B.; Patra, S.; Fiedler, J.; Sunoj, R. B.; Janardanan, D.; Lahiri, G. K.; Kaim, W. *J. Am. Chem. Soc.* **2008**, 130, 3532–3542.
- (17) (a) Krejcik, M.; Danek, M.; Hartl, F. *J. Electroanal. Chem. Interfacial Electrochem.* **1991**, 317, 179–187. (b) Kaim, W.; Fiedler, J. *Chem. Soc. Rev.* **2009**, 38, 3373–3382.
- (18) Burla, M. C.; Caliandro, R.; Camalli, M.; Carrozzini, B.; Casciaro, G. L.; Caro, L. De; Giacovazzo, C.; Polidori, G.; Siliqi, D.; Spagna, R. *SIR2008*; Institute of Crystallography: Bari, Italy, 2007.
- (19) (a) Sheldrick, G. M. *Acta Crystallogr., Sect. A: Found. Crystallogr.* **2008**, 64, 112–122. (b) *Program for Crystal Structure Solution and Refinement*; University of Göttingen: Göttingen, Germany, 1997.
- (20) Lee, C.; Yang, W.; Parr, R. G. *Phys. Rev. B: Condens. Matter Mater. Phys.* **1988**, 37, 785–789.
- (21) (a) Andrae, D.; Haeussermann, U.; Dolg, M.; Stoll, H.; Preuss, H. *Theor. Chim. Acta* **1990**, 77, 123–141. (b) Fuentealba, P.; Preuss, H.; Stoll, H.; Szentpaly, L. V. *Chem. Phys. Lett.* **1982**, 89, 418–422.
- (22) Frisch, M. J.; Trucks, G. W.; Schlegel, H. B.; Scuseria, G. E.; Robb, M. A.; Cheeseman, J. R.; Scalmani, G.; Barone, V.; Mennucci, B.; Petersson, G. A.; Nakatsuji, H.; Caricato, M.; Li, X.; Hratchian, H. P.; Izmaylov, A. F.; Bloino, J.; Zheng, G.; Sonnenberg, J. L.; Hada, M.; Ehara, M.; Toyota, K.; Fukuda, R.; Hasegawa, J.; Ishida, M.; Nakajima, T.; Honda, Y.; Kitao, O.; Nakai, H.; Vreven, T.; Montgomery, J. A., Jr.; Peralta, J. E.; Ogliaro, F.; Bearpark, M.; Heyd, J. J.; Brothers, E.; Kudin, K. N.; Staroverov, V. N.; Kobayashi, R.; Normand, J.; Raghavachari, K.; Rendell, A.; Burant, J. C.; Iyengar, S. S.; Tomasi, J.; Cossi, M.; Rega, N.; Millam, J. M.; Klene, M.; Knox, J. E.; Cross, J. B.; Bakken, V.; Adamo, C.; Jaramillo, J.; Gomperts, R.; Stratmann, R. E.; Yazyev, O.; Austin, A. J.; Cammi, R.; Pomelli, C.; Ochterski, J. W.; Martin, R. L.; Morokuma, K.; Zakrzewski, V. G.; Voth, G. A.; Salvador, P.; Dannenberg, J. J.; Dapprich, S.; Daniels, A. D.; Farkas, O.; Foresman, J. B.; Ortiz, J. V.; Cioslowski, J.; Fox, D. J. *Gaussian 09*, revision A.02; Gaussian, Inc.: Wallingford, CT, 2009.
- (23) (a) Bauernschmitt, R.; Ahlrichs, R. *Chem. Phys. Lett.* **1996**, 256, 454–464. (b) Stratmann, R. E.; Scuseria, G. E.; Frisch, M. J. *J. Chem. Phys.* **1998**, 109, 8218–8225. (c) Casida, M. E.; Jamorski, C.; Casida, K. C.; Salahub, D. R. *J. Chem. Phys.* **1998**, 108, 4439–4450.
- (24) (a) Barone, V.; Cossi, M. *J. Phys. Chem. A* **1998**, 102, 1995–2001. (b) Cossi, M.; Barone, V. *J. Chem. Phys.* **2001**, 115, 4708–4718. (c) Cossi, M.; Rega, N.; Scalmani, G.; Barone, V. *J. Comput. Chem.* **2003**, 24, 669–681.
- (25) Leonid, S. *Chemissian 1.7*, 2005–2010. Available at <http://www.chemissian.com>.
- (26) Zhurko, D. A.; Zhurko, G. A. *ChemCraft 1.5*; Plimus: San Diego, CA. Available at <http://www.chemcraftprog.com>.